Moment tensor analysis of the acoustic emission source in the rock damage process*

YU Huaizhong[1,2**], ZHU Qingyong[3], YIN Xiangchu[2,4] and WANG Yucang[5]

(1. State Key Laboratory of Earthquake Dynamics, Institute of Geology, China Earthquake Administration, Beijing 100029, China; 2. State Key Laboratory of Nonlinear Mechanics, Institute of Mechanics, Chinese Academy of Sciences, Beijing 100080, China; 3. School of Mathematics and Computational Science, Zhongshan University, Guangzhou 510275, China; 4. Center for Analysis and Prediction, China Seismological Bureau, Beijing 100036, China; 5. Quakes, Department of Earth Science, University of Queensland, Brishbane, Austrialia)

Received November 26, 2004; revised January 27, 2005

Abstract To further investigate the mechanism of acoustic emission (AE) in the rock fracture experiment, moment tensor analysis was carried out. The AE sources characterized by crack sizes, orientations and fracture modes, are represented by a time-dependent moment tensor. Since the waveforms recorded by AE monitors correlate to the moment tensors, we prefer to select the P wave amplitude from the full-space Green's function of homogeneous and isotropic materials to determine the six independent components of the moment tensor. The moment tensor analysis was used to investigate the AE sources recorded in the experiment, and three types of micro-cracks were found, which are tensile mode, shear mode and mixture of the tensile and shear mode. In addition, the motion of micro-cracks was decided by eigenvectors of moment tensor. Results indicate that the moment tensor analysis may be used as a measurement to reflect the damage evolution of rock specimen.

Keywords: moment tensor, acoustic emission, rock fracture.

The failure of brittle heterogeneous media involves nucleation, growth and coalescence of micro-damages[1]. Thus, the acoustic emission (AE) generated due to deformations and micro-damages plays an important role in the study of the failure of brittle heterogeneous media. AE can be defined typically as a transient elastic wave generated by the rapid release of energy within a brittle heterogeneous media. As an important method to investigate the damage evolution, AE has been extensively studied[2—6]. Up to now, studies on AE have experienced the empirical stage and moved into the study of propagation of elastic waves.

The AE wave theory was developed early in the 1960s[7—10] by geophysicists when studying transient waves in layered media. Breckenridge et al.[11] were the first one to use the Lamb's solution to study AE waveforms. To interpret the signatures of certain acoustic emission events recorded in carefully controlled experiments, they applied the Lamb-Pekeris solution to the response of a half-space under a concentrated force. In fact, AE events are different from earthquakes due to the presence of tensile cracks. Thus, the method to distinguish shear-type and tensile-type cracks is indispensable for AE source research.

The related parameters of AE source such as crack sizes, motion orientations, fracture modes and time history of micro-cracks formation, are represented by a moment tensor, which consists of six independent components related to the elastic modulus of the material, orientation of crack surface and displacement vector of the crack. Elastic wave theory can be applied to analyze the AE events by moment tensor analysis. To determine the six independent components of a moment tensor, Green's functions of finite particular geometries are necessary, and solving an integral equation of convolution is required. For example, a technique known as deconvolution was proposed[12] on the basis of several procedures developed in the past, such as the mathematical modeling of AE sources[8], evaluation of Green's functions in bounded media[13], calibration of transducers[11,14], and deconvolution techniques[9,12,14,15]. After that, a simplified approximate method was de-

* Supported by National Natural Science Foundation of China (Grant Nos. 10232050, 4014019 and 10102024), the Ministry of Science and Technology of China (Grant No. 2002CCA04500) and the Computer Network Information Center of Chinese Academy of Sciences (Grant No. INF105-SCE-2-02)

** To whom correspondence should be addressed. E-mail: Yuhz@lnm.imech.ac.cn or Yuhz750216@sina.com

veloped in case that the complete Green's function was not available.

Here, we select another feasible method put forward by Ohtsu[6] to perform moment tensor analysis for AE sources of our experiment, since the method is easier to be operated.

1 Theory of moment tensor analysis

For an isotropic, linearly elastic solid material, the equations of motion are defined as

$$\mu \boldsymbol{u}_{i,jj}(x,t) + (\lambda + \mu)\boldsymbol{u}_{j,ji}(x,t) + \boldsymbol{f}_i(x,t) = \rho \frac{\mathrm{d}^2 \boldsymbol{u}_i(x,t)}{\mathrm{d}t^2}, \quad (1)$$

where $\boldsymbol{u}_i(x,t)$ and $\boldsymbol{f}_i(x,t)$ are displacement and body forces per unit volume at location x and time t, ρ is the mass density, λ, μ are lame constants.

Breckenridge et al.[11] found that Lamb solution of Navier's equation could be used to interpret the waveform of AE events. If the Lamb solution of Navier's equation was regarded as Green's function $\boldsymbol{G}_{ip}$, and the fractures of macro-cracks were taken as dislocation[16], which means acoustic emission by a micro-crack inside materials is modeled by a displacement discontinuity $\boldsymbol{b} = \boldsymbol{u}_+ - \boldsymbol{u}_-$ ($\boldsymbol{u}_+$ and $\boldsymbol{u}_-$ denote the displacement at surface of micro-crack S_+ and S_-, respectively), then the displacement at location x and time t could be expressed as

$$u_i(x,t) = \int_0^t \int_S \boldsymbol{T}_{ik}(x,y,t-\tau) b_k(y,\tau)\mathrm{d}S\mathrm{d}\tau. \quad (2)$$

Here, S is the surface of micro-crack ($S = S_+ + S_-$), and $\boldsymbol{T}_{ik}(x,y,t)$ is tensor derived from Green's function defined as

$$\boldsymbol{T}_{ik} = \boldsymbol{C}_{pqkl}\boldsymbol{G}_{ip,q}\boldsymbol{n}_l, \quad (3)$$

where the elastic constants $\boldsymbol{C}_{pqkl} = \lambda\boldsymbol{\delta}_{pq}\boldsymbol{\delta}_{kl} + \mu(\boldsymbol{\delta}_{pk}\boldsymbol{\delta}_{ql} + \boldsymbol{\delta}_{pl}\boldsymbol{\delta}_{qk})$, $\boldsymbol{G}_{ip,q}$ is the spatial derivative of Green's function, and $\boldsymbol{n}_l$ is the outward normal vector to the crack surface.

The dislocation $\boldsymbol{b}_k(y,t)$ in Eq.(2) contains the size, the motion direction and the time dependence function of crack formation. According to Ref. [8], it can be represented by a product of size $b(y)$, direction $\boldsymbol{l}_k$ and time function $s(t)$. Therefore, the displacement at location x can be written as

$$\boldsymbol{u}_i(x,t) = \int_0^t s(\tau)\int_S \boldsymbol{G}_{ip,q}(x,y,t-\tau) \cdot \boldsymbol{m}_{pq}(y)\mathrm{d}S\mathrm{d}\tau. \quad (4)$$

The tensor $\boldsymbol{m}_{pq}(y)$ is called moment tensor, which comprises the size and direction of micro-crack and can be expressed as

$$\boldsymbol{m}_{pq}(y) = \boldsymbol{C}_{pqkl} b(y) \boldsymbol{l}_k \boldsymbol{n}_l. \quad (5)$$

Supposing the dimension of ΔF is much smaller than the distance between the source and receiver, the micro-crack then can be approximated as a point source. Thus the displacement can be written as

$$\boldsymbol{u}_i(x,t) = \boldsymbol{m}_{pq} \cdot \Delta F \int_0^t s(\tau)\boldsymbol{G}_{ip,q}(x,y,t-\tau)\mathrm{d}\tau. \quad (6)$$

Using the full-space Green's function of homogeneous and isotropic material proposed by Ref. [8], the P wave portion was selected to determine the six independent moment tensor components by solving a set of linear algebraic equations,

$$A_P(x) = C\boldsymbol{f}_i r_i r_p r_q \boldsymbol{M}_{pq}(y)/R, \quad (7)$$

where $A_P(x)$ is the P wave amplitude at the sensor location x, R is the distance from AE sources y to the sensor x, and r_i is its direction cosine, $\boldsymbol{f}_i$ is the direction vector of the sensor face, C is the common factor, and $\boldsymbol{M}_{pq} = m_{pq} \cdot \Delta F$.

2 AE experiment and moment tensor analysis

The rock specimen was subjected to both axial and lateral loads simultaneously. The lateral load was symmetrically applied to specimen with steel plates on the two smaller sides and was retained at a constant of 60 tons (the maximum of lateral load is 100 tons). The axial load was applied to the rock specimen with the ram controlled by a hydraulic valve (the maximum axial load is 500 tons) (Fig. 1). The whole loading process was divided into four stages, with different load levels in each one. Between two consecutive stages, the load was thoroughly unloaded first and then reloaded to a new level. In every loading stage, the load was perturbed by triangular oscillations with the amplitude of 10 tons. Thus the three

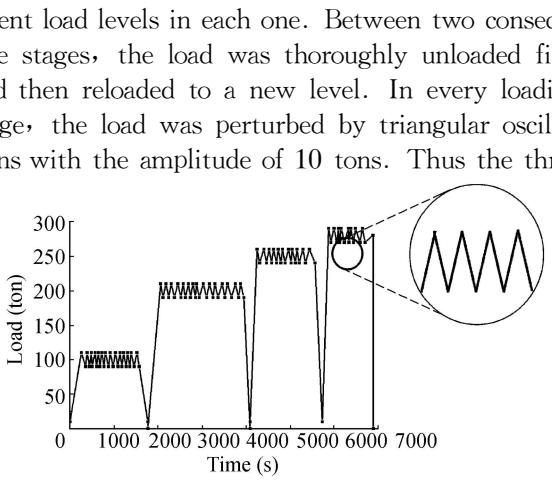

Fig. 1. The cycling stress history of the specimen.

principle stresses were not equal to each other. The tri-axial compression experiment involving rectangular prism of Wuding gneiss was conducted. The parameters of Wuding gneiss are: Young's modulus E = 27 GPa, Poisson ratio ν = 0.26, density $\rho = 2.6 \times 10^3$ kg/m^3, and compressional wave speed c = 3200 m/s.

The AE signals were recorded continuously using the "A-line 32D AE system" made by the A. F. Ioffe Physical Technical Institute, Russian Academy of Sciences and Interunis Ltd. Each channel consists of an AE sensor, a pre-amplifier and an AECB (acoustic emission channel board). In Fig. 2, ten piezoelectric AE sensors were attached directly to the rock specimen free surface ('o' represent the location of transducers), five on each side, which were used to monitor the sound waves generation from the specimen. Then the AE signals were converted into electrical signals which were amplified by a preamplifier and converted into a digital data stream in an AECB. AE features such as arrival times, rise-times, duration, peak amplitude, energy and counts were extracted by a FPGA (field programmable gate array). The frequency of input filter ranges from 10 kHz to 500 kHz [−3 dB] and 24 dB/octave[17]. The ADC (analogue to digital converter) was operated at a 5 MHz sampling frequency and provided a 16 bit resolution. The threshold values ranged from 45 to 51 dB and the resolution was 1 μV. The working frequency of the sensor ranged form 100 to 500 kHz and its sensitive factor on 1 7 5 kHz was 6 7 dB relative to 1 B / m . AE events were positioned in real time and could be displayed on a screen and recorded for post-processing. The absolute error[2—4] of AE event locations was less than 10 mm[17—19]. While these features were extracted, the complete waveform can also be recorded, whose amplitude data can be applied to determine the moment tensor components. Six AE events of first load stage whose motions were recorded clearly were chosen for moment tensor analysis. Similarly, four AE events were chosen for the second, third, and fourth load stages, respectively. The results are shown in Table 1, where $\boldsymbol{M}_{ij}(i,j=1,2,3)$ are six independent components, Coordi (mm) is the location of the event, and λ_1, λ_2, λ_3 are three eigenvalues of moment tensors.

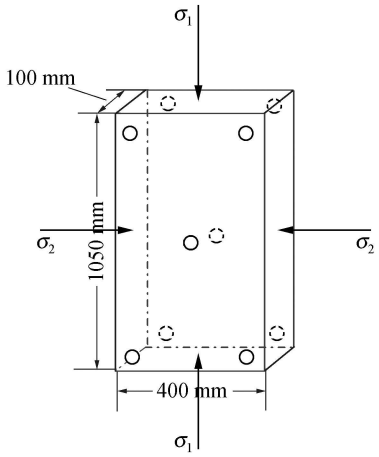

Fig. 2. The geometry of the specimen, the loading conditions, and the arrangement of AE sensors (circles).

Table 1. Six components of moment tensor for micro-cracks

Stage	Event	Coordi (mm)	M_{11}	M_{12}	M_{13}	M_{22}	M_{23}	M_{33}	λ_1	λ_2	λ_3
1	2	(92,614,370)	0.602	0.452	0.091	−0.614	0.120	1.000	1.055	0.701	−0.768
	9	(14,31,147)	0.682	−0.354	0.327	0.940	0.571	1.000	1.781	0.443	0.398
	17	(70,22,300)	−0.020	−0.130	−0.150	0.820	0.600	1.000	1.542	0.303	−0.045
	21	(73,35,257)	0.820	−0.243	−0.462	0.311	0.314	1.000	1.512	0.440	0.179
	29	(53,18,259)	0.221	0.511	−0.271	−0.312	0.646	1.000	1.268	0.519	−0.878
	36	(38,55,144)	0.921	−0.677	0.571	0.736	−0.241	1.000	1.904	0.664	0.089
2	27	(96,932,82)	0.738	0.400	0.102	−0.603	−0.490	1.000	1.138	0.845	−0.848
	41	(95,123,300)	−0.104	−0.339	−0.011	1.000	0.431	0.181	1.259	0.057	−0.239
	47	(82,892,71)	−0.011	−0.268	−0.080	1.000	0.395	−0.071	1.195	−0.075	−0.201
	63	(70,220,300)	0.489	0.351	0.076	−0.623	−0.601	1.000	1.200	0.578	−0.912
3	1	(83,944,29)	0.437	0.205	0.035	−0.125	−0.394	1.000	1.125	0.493	−0.306
	4	(90,961,61)	0.647	0.212	0.057	−0.097	−0.411	1.000	1.137	0.698	−0.285
	9	(80,982,18)	−0.300	0.221	0.016	−0.921	−0.610	1.000	1.179	−0.246	−1.154
	17	(68,877,37)	0.211	0.183	0.028	−0.421	−0.732	1.000	1.311	0.242	−0.764
4	6	(18,879,118)	0.522	0.197	0.045	−0.093	−0.366	1.000	1.112	0.574	−0.256
	13	(60,877,137)	0.428	0.233	0.050	−0.303	−0.456	1.000	1.144	0.487	−0.507
	19	(32,902,150)	0.736	0.196	0.055	0.055	−0.352	1.000	1.117	0.785	−0.111
	27	(44,904,197)	−0.053	0.188	0.018	−0.669	−0.556	1.000	1.169	−0.013	−0.879

After the moment tensor was determined, the eigenvalue decomposition was applied to classify the AE source into a tensile crack or a shear crack. To deal with the moment tensors, three kinds of decomposition were divided, specifically the double-couple (DC) part, the compensated linear vector dipole (CLVD) part, and the isotropic part. The way of classification is to determine the major contribution of the tensile crack and the shear crack by taking into account proportions of DC part (X), CLVD part (Y), and isotropic part (Z)[20]. Relative proportions of X, Y, and Z are determined by

$$\begin{aligned}\frac{\lambda_1}{\lambda_1} &= X + Y + Z,\\ \frac{\lambda_2}{\lambda_1} &= 0 - 0.5Y + Z,\\ \frac{\lambda_3}{\lambda_1} &= -X - 0.5Y + Z,\end{aligned} \tag{8}$$

where λ_1 is the maximum eigenvalue, λ_2 is the intermediate eigenvalue, and λ_3 is the minimum eigenvalue of the moment tensor. The ratio of X to $(Y+Z)$ can determine the type of AE source. If the ratio is larger than 50%, the AE source can be regarded as a shear crack. But if the ratio is lower than 50%, the AE source can be looked as a tensile crack. To classify the crack type from moment tensor components, the eigenvalues were decomposed (X, Y, Z) (Table 2).

Table 2. The decomposition of eigenvalues of the moment tensor and the type of AE sources

Stage	Event	X	Y	Z	Type of crack
1	2	1.392	−0.705	0.312	Shear
	9	0.025	0.484	0.491	Tensile
	17	0.226	0.385	0.389	Tensile
	21	0.409	0.200	0.391	Shear & tensile
	29	1.102	−0.341	0.239	Shear
	36	0.302	0.233	0.465	Tensile
2	27	1.488	−0.820	0.332	Shear
	41	0.235	0.480	0.285	Tensile
	47	0.105	0.638	0.256	Tensile
	63	1.241	−0.482	0.240	Shear
3	1	0.710	−0.099	0.389	Shear
	4	0.865	−0.319	0.454	Shear
	9	0.770	0.292	−0.062	Shear
	17	0.767	0.032	0.201	Shear
4	6	0.747	−0.176	0.429	Shear
	13	0.869	−0.196	0.327	Shear
	19	0.802	−0.337	0.535	Shear
	27	0.741	0.180	0.079	Shear

Three eigenvectors of the moment tensor $\boldsymbol{M}_{pq}$ corresponding to three eigenvalues can be represented by the direction of crack motion $\boldsymbol{l}$ and unit normal $\boldsymbol{n}$ as

$$\boldsymbol{v}_1 = \boldsymbol{l} + \boldsymbol{n}, \quad \boldsymbol{v}_2 = \boldsymbol{l} \times \boldsymbol{n}, \quad \boldsymbol{v}_3 = \boldsymbol{l} - \boldsymbol{n}, \tag{9}$$

where the eigenvector $\boldsymbol{v}_1$ directs the motion of the crack opening in tensile crack. For shear crack, the direction of crack motion vector $\boldsymbol{l}$ or the unit normal vector $\boldsymbol{n}$ can be determined from the sum and deduct of eigenvector $\boldsymbol{v}_1$ and $\boldsymbol{v}_3$. Table 3 shows the motion of AE sources determined by using eigenvectors of the moment tensors (θ and φ are shown in Fig. 3).

Table 3. The orientations of cracks motion for AE sources

Stage	Event	θ(°)	φ(°)
1	2	50.9	39.7
	9	133.5	34.1
	17	130.7	11.0
	21	113.1(tensile) 159.8(shear)	62.4(tensile) 19.1(shear)
	29	70.4	41.1
	36	47.9	53.1
2	27	30.0	10.3
	41	157.9	14.2
	47	161.9	13.7
	63	27.5	8.7
3	1	28.5	10.3
	4	27.3	9.2
	9	29.7	10.0
	17	24.3	6.6
4	6	28.9	10.5
	13	28.3	9.8
	19	27.4	9.5
	27	28.9	8.3

3 Discussion

Results of the eigenvalue analysis of the moment tensors and the unified decomposition have been shown in Table 2. From the values of X ratio, the events were classified into either tensile cracks or shear cracks, except for event 21 during the first load process whose X ratio is between 40% and 50%, and a crack mixture of tensile type and shear type was analyzed. The classification of crack types is a necessary procedure to determine the motion of micro-cracks. To tensile cracks, the motion orientations are determined as the direction of the first eigenvector. To shear cracks, the motion orientations are determined from the sum of the first and the third eigenvectors. The motion orientations are represented by θ and φ, as shown in Fig. 3. Angle θ on y-z plane, measured from the y-axis to z-axis, and angle φ on x-y plane, measured from the x-axis to y-axis, are listed in Table 3, and Table 4 is the maximum, minimum and average values of angles θ, φ within different load stages. When the axial load was at a low level, the motion orientations were scattered, whereas with the

increasing of axial load, the motion orientations of micro-cracks were in remarkable agreement. These results correspond to the 3-D AE sources location process of Ref. [18].

Table 4. The maximum, minimum and average values of angles θ, φ within different stages

Stage	θ_{max}(°)	θ_{min}(°)	θ_{aver}(°)	φ_{max}(°)	φ_{min}(°)	φ_{aver}(°)
1	159.8	47.9	100.9	62.4	11.0	37.2
2	161.9	27.5	94.3	14.2	8.7	11.7
3	29.7	24.3	27.5	10.3	6.6	9.0
4	28.9	27.4	28.4	10.5	8.3	9.5

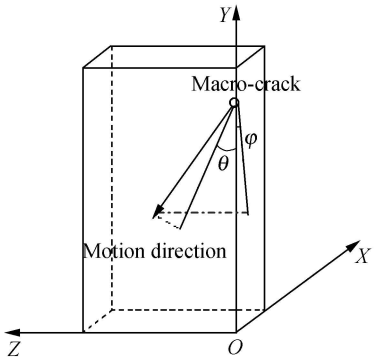

Fig. 3. Motion orientation of the AE source.

4 Conclusion

The moment tensor analysis not only is a reasonable method to study type and motion of micro-cracks, but also can reflect quantitatively the damage evolution of rock specimen. Selecting the P wave amplitude from the full-space Green's function of isotropic materials is a feasible way to compute the six independent components of the moment tensor. In this paper, although only finite AE events were analyzed, results show that the micro-cracks within rock specimen could be revealed by moment tensor analysis. There were shear and tensile cracks observed in the experiment. When the axial load was at the low levels, more than half of cracks were tensile. With the increasing of axial load, the proportion of this type decreased, but the proportions of shear type increased. These results imply that the tensile cracks occur prior to shear cracks, which can confirm the fact that although some cracks start from tensile type first, the opening of seams will allow shear motions along the fracture surface. Then shear cracks will play a dominant role in rock fracture process, which corresponds to the shear fracture of rock specimen. On the other hand, with the increasing of axial load, the harmonic change of motion orientations was observed. Thus, based on the motion orientations of crack, we can imply the tendency of damage evolution and may predict the macro-fracture of rock specimen. Therefore, the moment tensor analysis of AE source may be used as a new technique to predict the failure of heterogeneous media.

References

1 Krajcinovic D. Damage Mechanics, 1st ed. North-Holland Elsevier Amsterdam: Netherlands Press, 1996, 1—774.
2 Lockner D. and Byerlee J. D. Hydrofracture in Weber sandstone at high confining pressure and differential stress. J. Geophys. Res. 1977, 82(14): 2018—2026.
3 Lockner D. A., Byerlee J. D., Kuksenko V. et al. Quasi-static fault growth and shear fracture energy in granite. Nature, 1991, 350(7): 39—42.
4 Lockner D. A. The role of emission in the study of rock failure. Int. J. Rock Mech. Min. Sci. & Geomech. Asstr., 1993, 30(7): 883—899.
5 Ohtsu M. Source mechanism and waveform analysis of acoustic emission in concrete. J. Acoust. Emission, 1982, 1(2): 103—112.
6 Ohtsu M. Simplified moment tensor analysis and unified decomposition of AE. J. Geophys. Res., 1991, 95: 6211—6221.
7 Maruyama T. On force equivalents of dynamic elastic dislocations with reference to the earthquake mechanism. Bull. Earthquake Res. Inst. Univ. Tokyo, 1963, 41: 467—486.
8 Aki K. and Rechards P. G. Quantitative Seismology: Theory and Methods, 1st ed. San Francisco: W. H. Freeman Cooper Press, 1980, 1—932.
9 Stump B. W. and Johnson L. R. The determination of source properties by the linear inversion of seismograms. Bull. Seis. Soc. Am., 1977, 67: 1489—1502.
10 Kanamori H. and Given J. W. Use of long-period surface waves for fast determination of earthquake sources parameters. Phys. Earth. Planet. Inter., 1981, 27: 8—31.
11 Breckenridge F. R., Tschiegg C. E. and Greespan M. Acoustic emission: some applications of Lamb's problem. J. Acoust. Soc. Am., 1975, 57(3): 626—631.
12 Michael J. E. and Pao Y. H. The inverse source problem for an oblique force on an elastic plate. J. Acoust. Soc. Am., 1985, 77: 2005—2011.
13 Ceranoglu A. and Pao Y. H. Propagation of elastic pulses and acoustic emission in a plate, parts I, II, and III. ASME J. Appl. Mech., 1981, 48: 125—147.
14 Hsu N. N., Simmons A. and Hardy S. C. An approach to acoustic emission signal analysis. Mater. Eval., 1977, 35: 100—106.
15 Michaels J. E., Michaels T. E. and Sachse W. Applications of deconvolution to microseismic signal analysis. Mater. Eval., 1981, 39: 1032—1036.
16 Eshelby J. D. Dislocation theory for geophysical applications. Phil. Trans. R. Soc. London, 1973, A274: 331—338.
17 Yin X. C., Yu H. Z., Kukshenko V. et al. Load-unload response ratio (LURR), accelerating energy release (AER) and state vector evolution as precursors to failure of rock specimens. Pure Appl. Geophys., 2004, 161(11/12): 2405—2416.
18 Yu H. Z., Yin X. C., Liang N. G. et al. Experimental research on the load/unload response ratio theory. Earthquake Research in China, 2003, 17(3): 227—235.
19 Yu H. Z., Yin X. C., Liang N. G. et al. Experimental research on the critical point hypothesis. Acta Seismologic Sinica, 2004, 17 (sup.): 129—137.
20 Feignier B. and Young R. P. Moment tensor inversion of induced microseismic events evidence of nonshear failures in the $-4<M<-2$ moment magnitude range. Geophysical Research Letters, 1992, 19(14): 1503—1506.